Journal of Alloys and Compounds 509 (2011) 2897–2902

Contents lists available at ScienceDirect

Journal of Alloys and Compounds

journal homepage: www.elsevier.com/locate/jallcom

Temperature dependent admittance spectroscopy of GaAs/AlGaAs single-quantum-well laser diodes (SQWLDs)

A. Bengi[a], H. Uslu[a,*], T. Asar[a], Ş. Altındal[a], S.Ş. Çetin[a], T.S. Mammadov[a,b], S. Özçelik[a]

[a] Physics Department, Faculty of Arts and Sciences, Gazi University, Ankara, Turkey
[b] National Academy of Science, Institute of Physics, Baku, AZ 1143, Azerbaijan

ARTICLE INFO

Article history:
Received 12 August 2010
Received in revised form
17 November 2010
Accepted 22 November 2010
Available online 30 November 2010

Keywords:
QW lasers
C–V–T characteristics
Barrier height
Series resistance

ABSTRACT

In this study, the main electrical parameters, such as doping concentration (N_D), barrier height (Φ_{CV}), depletion layer width (W_D), series resistance (R_s) and Fermi energy level (E_F), of GaAs/$Al_xGa_{1-x}As$ single quantum well (SQW) laser diodes were investigated using the admittance spectroscopy (C–V and G/ω–V) method in the temperature range of 80–360 K. The reverse bias C^{-2} vs. V plots gives a straight line in a wide voltage region, especially in weak inversion region. The values of Φ_{CV} at the absolute temperature (T = 0 K) and the temperature coefficient (α) of barrier height were found as 1.22 eV and -8.65×10^{-4} eV/K, respectively. This value of α is in a close agreement with α of GaAs band gap (-5.45×10^{-4} eV/K). Experimental results show that the capacitance–voltage (C–V) and conductance–voltage (G/ω–V) characteristics of the diode are affected by not only temperature but also R_s. The capacitance–voltage–temperature (C–V–T) and conductance–voltage–temperature (G/ω–V–T) characteristics confirmed that temperature and R_s of the diode have effects on the electronic parameters in SQW laser diodes.

1. Introduction

Gallium arsenide (GaAs) based structures are extensively used as a basic component for high speed electronic, optoelectronic, low power devices and quantum-well (QW) detectors and lasers [1–8]. The GaAs well layers are doped with n-type dopant (Si) to provide electrons to the ground states of the wells. In these devices, the conduction mechanism depends on various parameters such as surface preparation process, formation of barrier height (BH) and interface states (N_{ss}) at M/S interface, doping carrier concentration in semiconductor (N_D or N_A), series resistance (R_s), substrate temperature and applied bias voltage [9–14]. Among them, R_s is effective only in the downward curvature region (accumulation region) of the C–V characteristics, but the N_{ss} is effective in weak inversion and depletion regions [15–20].

The obtained barrier height at M/S interface depends on the measurement methods. In general, there is a discrepancy between the BHs obtained from reverse bias C–V measurements and forward bias I–V measurements, i.e., the value of Φ_{CV} is significantly higher than Φ_{IV}. This discrepancy could be explained in terms of the existence of excess capacitance of devices due to N_{ss} or dislocations at M/S interface and barrier height (BH) inhomogeneties [21–28]. It is well known that the electrical characterization only at room temperature or narrow temperature range of the semiconductor devices, such as metal–semiconductor (MS) or metal–insulator–semiconductor (MIS) type Schottky barrier diodes (SBDs), solar cells (SCs) and laser diodes (LDs), cannot give detailed information about their conduction mechanisms or the nature of barrier formation at M/S interface. However, the temperature dependent I–V and C–V measurements allow us to understand the different aspects of conduction mechanisms of these devices [29–34].

Therefore, the C–V and G/ω–V measurements should be done over a wide temperature range in order to clearly understand the nature of BH and conduction mechanisms. The temperature dependence of electrical characteristics of these devices has been widely investigated in the literature [35–46]. In our previous work [20], we have investigated temperature and voltage dependent current transport mechanisms in GaAs/AlGaAs single-quantum-well lasers using forward and reverse bias I–V measurements in the temperature range of 80–360 K. The analysis of the experimental I–V data of the studied structures indicated that the current-transport was controlled by the Thermionic Field-Emission (TFE) mechanism below 170 K and Thermionic Emission (TE) mechanism above 200 K. The high values of n especially at low temperatures showed that the conduction is controlled by TFE [7,20]. These results confirm that the predominant current transport mechanism is not only the thermionic emission mechanism. In this study, the first aim is to investigate the temperature dependent Φ_{CV} and R_s obtained from C–V and G/ω–V measurements, and compare with previous study (obtained from I–V measurements) in GaAs/$Al_xGa_{1-x}As$ single quantum well (SQW) laser diodes. The second aim is to explain

* Corresponding author. Tel.: +90 312 202 11 31; fax: +90 0312 212 22 79.
E-mail address: h.uslu@gazi.edu.tr (H. Uslu).

0925-8388/$ – see front matter © 2010 Elsevier B.V. All rights reserved.
doi:10.1016/j.jallcom.2010.11.150

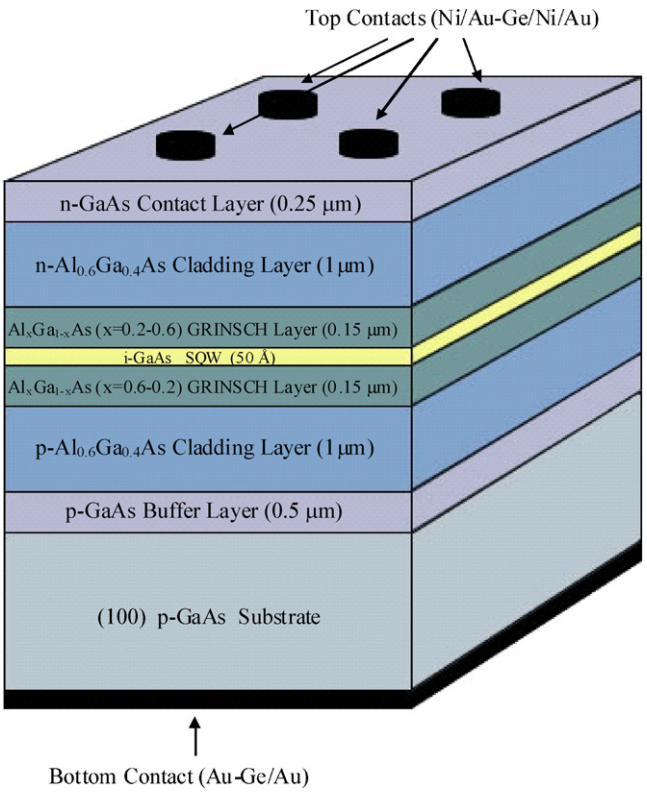

Fig. 1. Schematic diagram for the GaAs/$Al_xGa_{1-x}As$ SQW laser diode.

the discrepancy in barrier height obtained from reverse bias *C–V* and forward bias *I–V* measurements. In addition, the temperature dependence of reverse and forward bias *C–V* and G/ω–*V* characteristics of GaAs/$Al_xGa_{1-x}As$ SQW laser diodes by considering R_s effect in the temperature range of 80–360 K.

2. Experimental details

The GaAs/$Al_xGa_{1-x}As$ single quantum well (SQW) laser was grown on Zn doped p-type GaAs (1 0 0) substrate by solid source V80H molecular beam epitaxy (MBE) system. Prior to growth of the SQW laser structure, the substrate was cleaned conventionally using acetone, methanol and deionized water. After the cleaning step, the substrate were mounted on the molybdenum free substrate holder and loaded into the system using fast entry lock. The substrate was transferred to outgas stage and heated up to 400 °C for 2 h to ensure the removal of any residual organics. After the outgas process, the substrate was transferred to deposition chamber and mounted on the manipulator. Then, the substrate was heated up to 690 °C for the oxide desorption. After observing the fully oxide desorption, the substrate temperature was reduced to 660 °C. After reducing the substrate temperature, 0.5 μm Be doped ($p_{Be} = 1 \times 10^{18}$ cm^{-3}) p-type GaAs buffer layer was grown at a constant growth rate of 2.780 Å/s. The active layer was sandwiched between 1 μm Si doped ($n_{Si} = 5 \times 10^{17}$ cm^{-3}) n-type and Be doped ($p_{Be} = 1 \times 10^{18}$ cm^{-3}) p-type $Al_{0.6}Ga_{0.4}As$ cladding layers and composed of 50 Å thickness single intrinsic i-GaAs quantum well layer and 150 Å thickness $Al_xGa_{1-x}As$ ($x = 0.20$–0.60) continuously graded-index separate-confinement-heterostructure (GRINSCH) barrier layers. Cladding, quantum well and barrier layers were grown at a constant growth rate of 0.447 Å/s for AlAs and 0,670 Å/s for GaAs. Finally, 0.25 μm heavily Si doped ($n_{Si} = 1 \times 10^{18}$ cm^{-3}) n-type GaAs contact layer was then grown at 660 °C at a constant rate of 2.780 Å/s to complete the growth. Fig. 1 shows the whole GaAs/$Al_xGa_{1-x}As$ SQW laser structure of the processed device.

For the electrical characterization of the device, the top (rectifier) and bottom (ohmic) contacts were formed by deposition of metals using thermal evaporation system (Bestec, Germany) having base pressure on the order of 10^{-8} mbar. The evaporating system has four crucibles for metal sources. After the small pieces of Au, Ni metals and Au–Ge alloy were loaded in the different crucibles at the same time, the deposition chamber was pumped to reach the desired base pressure. To form the bottom contact, firstly, Au–Ge alloy with the thicknesses of 1000 Å was deposited at 400 °C substrate temperatures with a growth rate of 2.4 Å/s. Secondly, Au metals with the thicknesses of 600 Å were deposited on the Au–Ge contact with a growth rate of 2.2 Å/s. After the formation of bottom contact the 1 mm diameter dot shaped multilayer top contact with the metal layer thicknesses of 350/500/350/1750 Å were formed by deposition of Ni/Au–Ge/Ni/Au metals with growth rates of 6.0/2.0/2.0/3.6 Å/s, respectively. After the top and bottom metallization processes, the sample was annealed at 425 °C for 25 s in a nitrogen ambient atmosphere in order to form the ohmic contacts. Then, the silver paste was used to connect wires to the sample in order to prepare it for *C–V* and G/ω–*V* measurements.

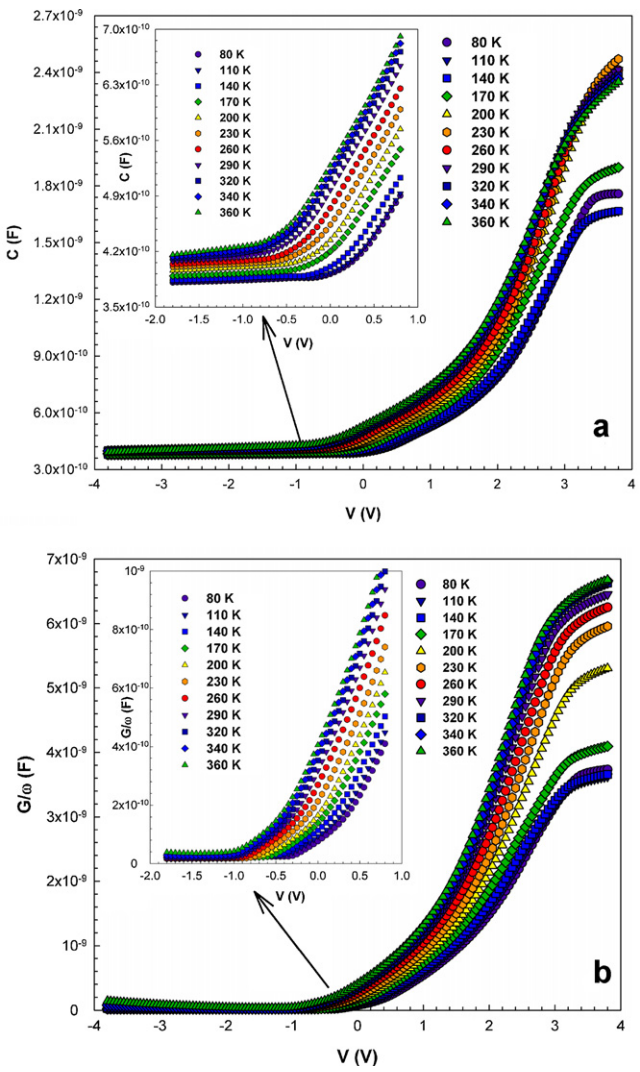

Fig. 2. The temperature dependent plots of: (a) *C–V* and (b) G/ω–*V* characteristics for the GaAs/$Al_xGa_{1-x}As$ SQW laser diode.

The *C–V* measurements of GaAs/$Al_xGa_{1-x}As$ single quantum well (SQW) laser diodes were carried out at enough high frequency (1 MHz) by using HP 4192A LF impedance analyzer in the temperature range of 80–360 K in a temperature controlled Janis vpf-475 cryostat, which enables us to make measurements in the temperature range of 77–450 K. The sample temperature was always monitored by using a copper–constantan thermocouple close to the sample, and measured with a dmm/scanner Keithley model 199 and a Lake Shore model 321 auto-tuning temperature controllers with sensitivity better than ±0.1 K. All measurements were carried out with the help of a microcomputer through an IEEE-488 ac/dc converter card.

3. Results and discussion

The temperature dependent reverse and forward bias *C–V* and G/ω–*V* characteristics of the GaAs/$Al_xGa_{1-x}As$ single quantum well (SQW) laser diodes at 1 MHz are shown in Fig. 2(a) and (b), respectively. As it can be seen in Fig. 2(a) and (b) both the *C–V* and the G/ω–*V* plots increase with the increasing temperature, especially in the depletion and accumulation regions. Also, it can be seen in Fig. 2(a) that *C–V* plots show a concave curvature behavior especially at low temperature in the accumulation region because of

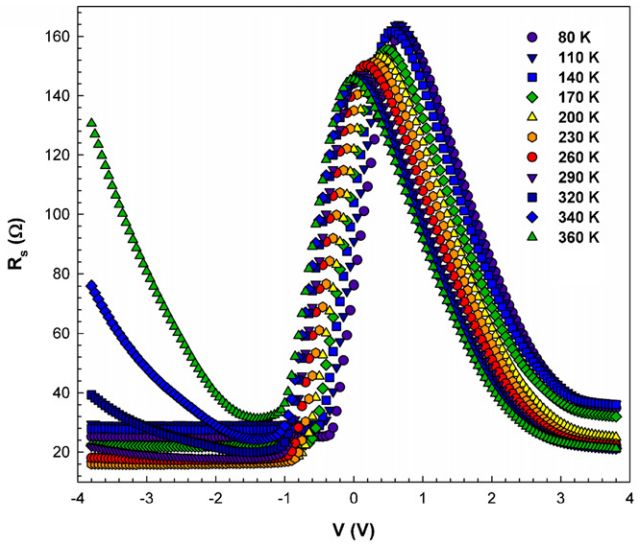

Fig. 3. The temperature dependence of series resistance as a function of applied bias voltage for the GaAs/Al_xGa_{1-x}As SQW laser diode.

the effect of R_s and interfacial insulator layer. It is clear that at high temperature, these peaks disappear. In order to extract the R_s of structure, several methods have been suggested in the literature [9,19,28]. Among them, the methods given in Refs. [34,47] are related to forward bias current–voltage characteristics. The other method which is given in Ref. [7] is related with the forward bias C–V and G/ω characteristics, and in addition, it can be generalized for whole measured region. In our calculations, we have applied the method developed by Nicollian and Brews [9].

When the C–V and G/ω–V plots are obtained at sufficiently high frequencies ($f \geq 500$ kHz), the effect of interface states (N_{ss}) can be eliminated, since they do not follow ac signal above these frequency values. In this case, the series resistance seems to be the most important parameter which causes the electrical characteristics of the semiconductor devices to be nonideal [9]. Therefore, in order to determine the real C and G/ω of these devices, the measured capacitance and conductance values, under reverse and forward bias, were corrected as C_c and G_c/ω by eliminating the effect of R_s. These very significant values require that special attention should be given to the effect of the series resistance in the applications of the admittance-based measured method. At sufficiently high frequency values, the values of R_s can be obtained from the C–V–T and G/ω–V–T measurements for a given applied bias voltage as [9,10]

$$R_s = \frac{G_m}{G_m^2 + (\omega C_m)^2} \tag{1}$$

where C_m and G_m represent the measured capacitance and conductance for any bias voltage at sufficiently high frequency values ($f \geq 500$ kHz). The values of R_s are calculated according to Eq. (1) and shown in Fig. 3 for various temperature values. These are significant values such that special attention should be given to effect of the R_s on the capacitance and conductance based measurements. It is clearly seen in Fig. 3 that the R_s plots give a peak. While the position of the peak shifts toward negative bias region, the amplitude of these peaks decreases with the increasing temperature. Such behavior of R_s–V peak can be attributed to the restructuring and reordering of interface charges.

In order to see the R_s effect, C–V and G/ω–V measurements at 1 MHz under the reverse and forward bias were corrected. The values of corrected capacitance C_c and conductance G_c are calculated

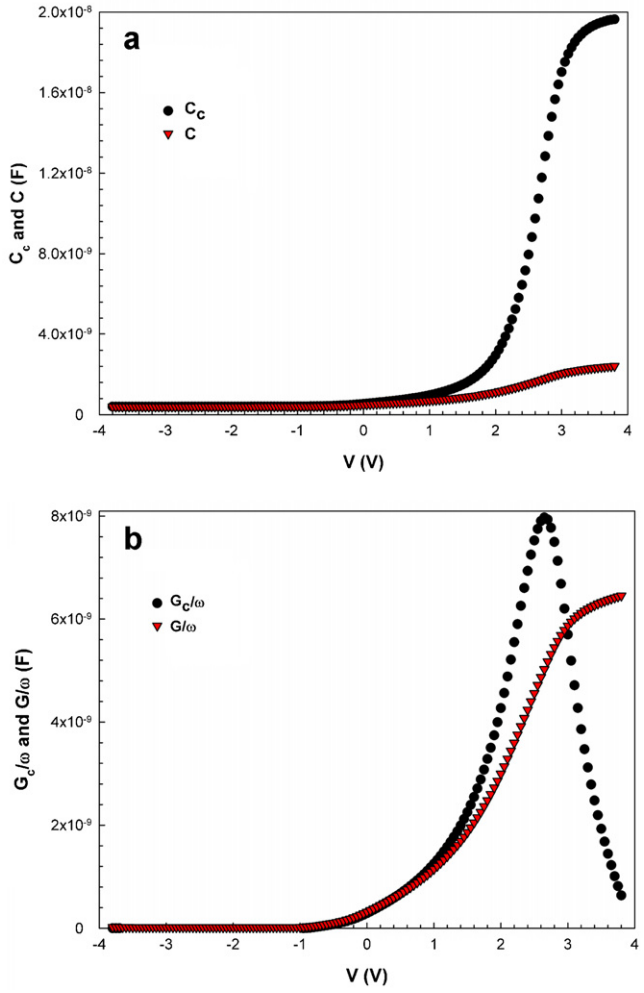

Fig. 4. The voltage dependent plot of the corrected (a) C_c–V and C–V (b) Gc/ω and G/ω–V for the GaAs/Al_xGa_{1-x}As SQW laser diode.

from the relations [9]

$$C_c = \frac{\left(G_m^2 + (\omega C_m)^2\right) C_m}{a^2 + (\omega C_m)^2} \tag{2}$$

and

$$C_c = \frac{\left(G_m^2 + (\omega C_m)^2\right) a}{a^2 + (\omega C_m)^2} \tag{3}$$

where $a = G_m - (G_m^2 + (\omega C_m)^2)R_s$. C–V and G/ω–V plots before and after correction are given in Fig. 4(a) and (b), respectively. As it can be seen in Fig. 4(a) and (b), when the correction was made on the C–V plot, the values of C_c increase from depletion region to accumulation region. On the other hand, the plot of the corrected conductance (G_c/ω–V) gives a peak in the depletion region which proves that the charge transfer can take place through the interface. Therefore, we can say that R_s effect is very strong in the depletion and accumulation regions.

In order to see voltage dependent C, G/ω and R_s values, we obtained capacitance–temperature (C–T), conductance–temperature (G/ω–T) and series resistance–temperature (R_s–T) plots for various applied bias voltages at 1 MHz which are shown in Figs. 5(a), (b) and 6, respectively. It is clear that the values of C and G/ω almost increase with the increasing temperature for each bias voltage value. It is well known, when temperature is increased, the generation of

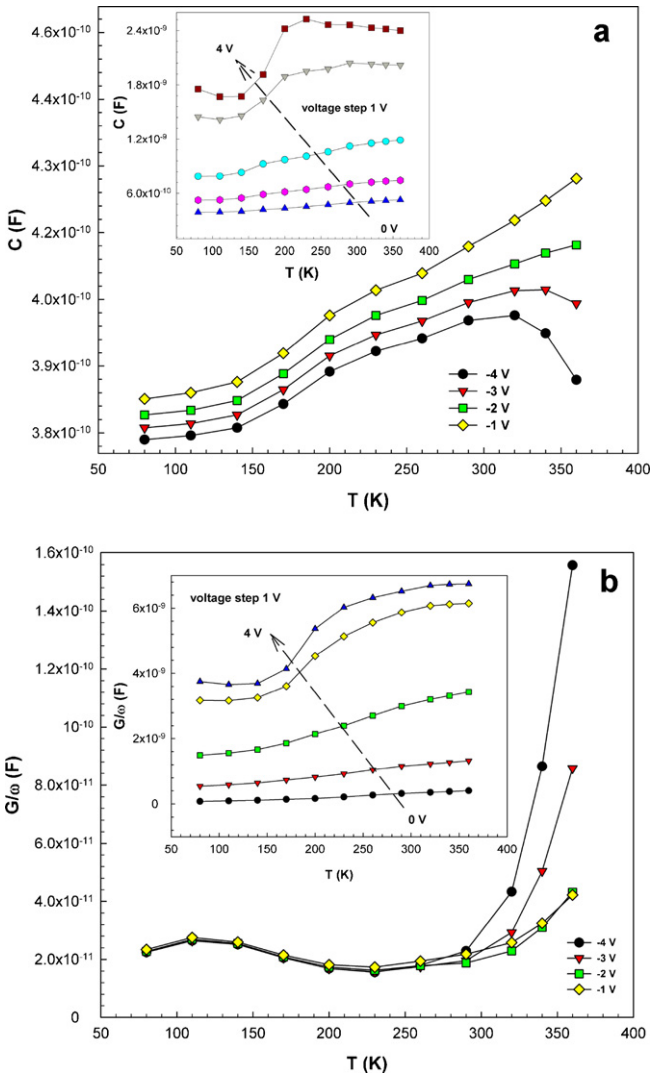

Fig. 5. The temperature dependence of (a) C and (b) G/ω values for the GaAs/Al_xGa_{1-x}As SQW laser diode for various bias voltages at 1 MHz.

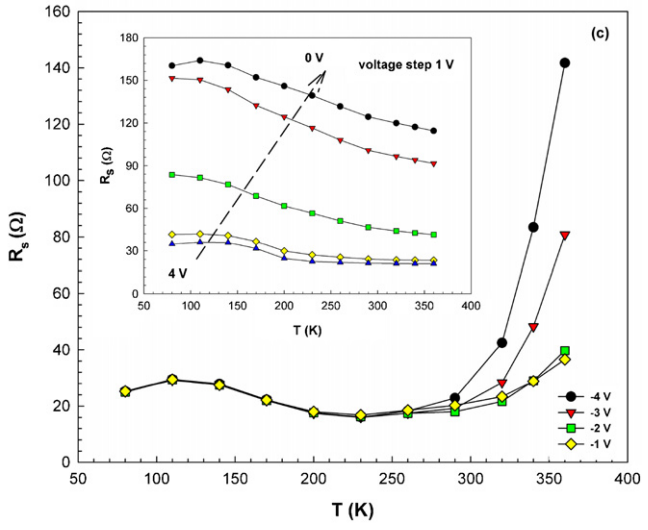

Fig. 6. The temperature dependence of R_s values for the GaAs/Al_xGa_{1-x}As SQW laser diode for various bias voltages at 1 MHz.

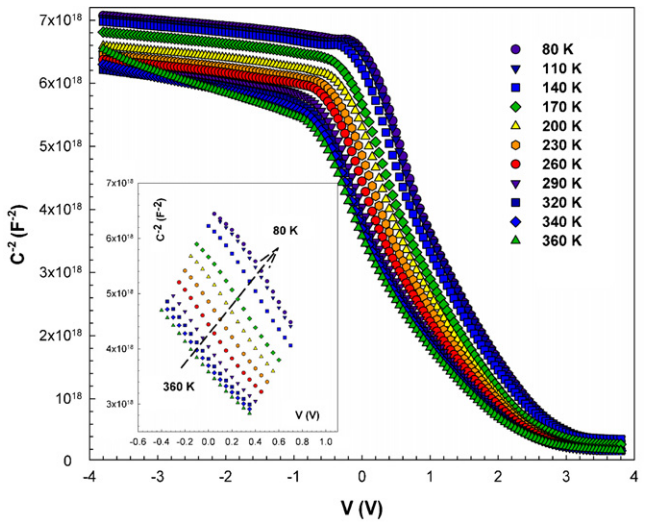

Fig. 7. The reverse bias C^{-2}–V characteristics of the GaAs/Al_xGa_{1-x}As SQW laser diode at various temperature and 1 MHz.

thermal carriers (electrons or holes) in semiconductor is enhanced both at positive and negative biased conditions. Therefore, the increase of C with temperature for almost all applied bias levels can be understood by charge storage (=Q/V). Therefore, in order to understand the effect of temperature on the capacitance (C) clearly, the temperature dependent capacitance and conductance measurements were performed in the temperature range of 80–360 K and the related graphs were given in Figs. 2 and 5.

As shown in Fig. 6 the values of R_s decrease with the increasing temperature for each bias voltage. Such behavior of C, G/ω and R_s with temperature can be attributed to the particular density distribution of N_{ss} and restructuring and reordering of interface charge at M/S interface with the increasing temperature.

The temperature dependent C^{-2} vs. V characteristics were presented in Fig. 7. As it can be seen from Fig. 7, the C^{-2} vs. V plot gives a straight line in a wide bias voltage range which is an evidence of the admittance measurements were done at sufficiently high frequency. The diffusion potential is obtained from the extrapolation of these straight lines to the voltage axis, and is given in Table 1. The depletion layer capacitance of diode can be expressed as [9–17].

$$C^{-2} = \frac{2(V_R + V_o)}{q\varepsilon_s N_D A^2} \tag{4}$$

where V_R is the reverse bias voltage, N_D is the doping concentration and V_o is the built-in voltage at zero bias, and can be determined from the extrapolation of the C^{-2} vs. V plot to the bias axis. Thus, the values of Fermi energy level (E_F), depletion layer width (W_D) and N_D were calculated at various temperatures from Fig. 7, and

Table 1
Temperature dependent values of various parameters determined from C–V characteristics of the GaAs/Al_xGa_{1-x}As SQW laser diode.

T (K)	N_D (cm^{-3})	E_F (meV)	W_D (cm)	Φ_{CV} (eV)	R_s (at 4 V) (Ω)
80	5.97×10^{16}	14	2.22×10^{-5}	1.17	34.83
110	5.83×10^{16}	20	2.24×10^{-5}	1.14	36.01
140	5.72×10^{16}	25	2.23×10^{-5}	1.10	35.78
170	5.92×10^{16}	30	2.10×10^{-5}	1.05	31.69
200	5.95×10^{16}	36	2.07×10^{-5}	1.04	24.65
230	6.19×10^{16}	40	1.96×10^{-5}	1.00	22.48
260	6.43×10^{16}	45	1.87×10^{-5}	0.99	21.86
290	6.60×10^{16}	49	1.79×10^{-5}	0.97	21.38
320	6.71×10^{16}	54	1.74×10^{-5}	0.95	21.02
340	6.82×10^{16}	57	1.70×10^{-5}	0.94	20.96
360	6.87×10^{16}	60	1.66×10^{-5}	0.92	20.96

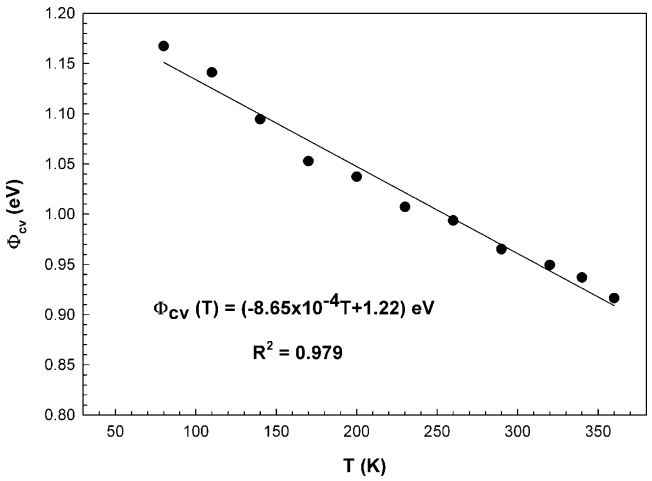

Fig. 8. The variation of Φ_{CV} as a function of temperature for the GaAs/$Al_xGa_{1-x}As$ SQW laser diode.

the following relations:

$$V_o = V_D - \frac{kT}{q} \tag{5}$$

where V_D is the diffusion potential at zero bias and E_F is the Fermi energy level which was obtained from

$$E_F = \frac{kT}{q} \ln\left(\frac{N_C}{N_D}\right) \tag{6}$$

with

$$N_C = 4.82 \times 10^{15}\, T^{3/2} \left(\frac{m_e^*}{m_o}\right)^{3/2} \tag{7}$$

where N_C is the effective density of states in the semiconductor conductance band and m_o is the rest mass of the electron. Thus, barrier height Φ_{CV} values were calculated at each temperature using the following relation:

$$\Phi_{CV} = V_o + \frac{kT}{q} + E_F - \Delta\Phi_B \tag{8}$$

where $\Delta\Phi_B$ is the image force barrier lowering and given by [48]

$$\Delta\Phi_B = \left(\frac{qE_m}{4\pi\varepsilon_s\varepsilon_o}\right)^{0.5} \tag{9}$$

where E_m is the maximum electric field and it is obtained from the following relation:

$$E_m = \left(\frac{2qN_DV_d}{\varepsilon_s\varepsilon_o}\right)^{0.5} \tag{10}$$

The obtained values of N_D, E_F, W_D, Φ_{CV} and R_s at different temperatures were presented in Table 1. As shown in Table 1, the obtained Φ_{CV}, W_D and R_s values decrease, while N_D and E_F values increase with the increasing temperature.

As can be seen in Fig. 8 and Table 1, the value of Φ_{CV} decrease with the increasing temperature and can be described as

$$\Phi_{CV}(T) = \Phi_{CV}(T=0) + \alpha T \tag{11a}$$

where Φ_{CV} (T = 0) is the barrier height extrapolated to zero temperature and α is the temperature coefficient of barrier height. In Fig. 8, the fitting of the Φ_{CV} (T) yields Φ_{CV} (T = 0) = 1.22 eV and $\alpha = -8.65 \times 10^{-4}$ eV/K. Here the negative temperature coefficient of the barrier height is in a close agreement with the temperature coefficient of the GaAs band gap (-5.405×10^{-4} eV/K) in the temperature range of interest. This temperature dependence of the barrier height can be explained in the terms of either Fermi level pinning or reduction of diffusion potential. The Fermi level can be pinned by either the metal induced gap states (MIGS) or defect states at the interface [29]. If the Fermi level is pinned by defects, the temperature dependence of barrier height will be weak because their ionization entropy changes slightly with temperature. If the Fermi level is pinned by defects, the temperature dependence of barrier height will be strong because the temperature dependence of the BH is governed by the temperature dependence of the band gap. As can be seen from Fig. 8 that the Φ_{CV} values decrease with the increasing temperature and this behavior can be attributed to the temperature dependence of GaAs Fermi level and band gap [7]. As a result, the variation of the barrier height with temperature is similar to forbidden band gap of semiconductor. It is well known the variation of band gap with temperature can be expressed approximately by a universal function [12]

$$E_g(T) = E_g(0\,\mathrm{K}) - \frac{\alpha T^2}{(\beta + T)} \tag{11b}$$

where E_g (0 K) is the value of band gap at absolute temperature, α is the negative temperature coefficient of band gap (dE_g/dT) and β is a constant. The decrease in the barrier height and band gap of semiconductor with the increasing temperature can be explained by using Eqs. (11a) and (11b), respectively.

4. Conclusions

The forward and reverse bias C–V and G/ω–V characteristics of the GaAs/$Al_xGa_{1-x}As$ SQW laser diode were measured in the temperature range of 80–360 K. The effects of R_s on the C–V and G/ω–V characteristics were investigated. Experimental results show that both C and G/ω values were quite sensitive to temperature, R_s and applied bias voltage, and they increase with the increasing temperature. The concave curvatures of C–V plots in the strong accumulation region and at low temperature have been attributed to the existence of R_s and interfacial insulator layer. As a result, the decrease in C and G/ω values was attributed to the lack of free charges especially at low temperature, carrier capture and emission of interface states, and the injection of charge carriers involving a process of hopping to localized interface traps. In addition, the values of Φ_{CV} obtained from C^{-2}–V plot decrease linearly with the temperature and the fitting of Φ_{CV} yields Φ_{CV} (T = 0) = 1.22 eV and $\alpha = -8.65 \times 10^{-4}$ eV/K. This negative temperature coefficient (α) of the barrier height is close to the GaAs band gap of 5.405×10^{-4} eV/K. In summary, it is obvious that neglecting the R_s and applied bias voltage effect on C–V and G/ω–V measurements can lead to very significant errors in the analysis of main diode parameters.

Acknowledgement

This work is supported by TUBITAK under the 108T018 project number.

References

[1] C.C. Lee, W.V. Chen, J. Park, Microelectron. J. 37 (2006) 1335.
[2] C.H. Chen, S.M. Baier, D.K. Arch, M.S. Shur, IEEE Trans. Electron. Dev. 35 (1988) 570.
[3] D.H. Kim, C.H. Roh, H.J. Song, Y.-S. Choi, C.-K. Hahn, H. Kim, J.H. Koh, T.G. Kim, Curr. Appl. Phys. 6 (S1) (2006) e172.
[4] M. Biber, Physica B 325 (2003) 138.
[5] C.S. Wu, C.P. Wen, R.N. Sato, M. Hu, C.W. Tu, J. Zhang, L.D. Flesner, L. Pham, P.S. Nayer, IEEE Trans. Electron. Dev. 39 (1992) 234.
[6] M. Kamp, J.P. Reithmaier, S. Reitzenstein, A. Forchel, Curr. Appl. Phys. 6 (S1) (2006) e166.
[7] A. Bengi, S. Altındal, S. Özçelik, S.T. Agaliyeve, T.S. Mammadov, Vacuum 83 (2009) 276.
[8] K. Zdansky, V. Gorodynskyy, J. Kosikova, A. Rudra, E. Kapon, D. Fekete, Semicond. Sci. Technol. 19 (2004) 897.
[9] E.H. Nicollian, J.R. Brews, MOS Physics and Technology, Wiley, New York, 1982.
[10] H. Kanbur, Ş. Altındal, A. Tataroğlu, Appl. Surf. Sci. 252 (2005) 1732.

[11] E.H. Rhoderick, R.H. Williams, Metal-Semiconductor Contacts, second ed., Clarendon Press, Oxford, 1988.
[12] S.M. Sze, Physics of Semiconductor Devices, third ed., John Wiley & Sons, New York, 2007.
[13] V. Saxena, K.S.V. Santhanam, Curr. Appl. Phys. 3 (2003) 227.
[14] M.E. Aydin, F. Yakuphanoglu, J.H. Eom, D.H. Hwang, Physica B 387 (2007) 239.
[15] M. Çakar, N. Yıldırım, Ş. Karataş, C. Temirci, A. Türüt, J. Appl. Phys. 100 (2006) 074505.
[16] C. Coskun, S. Aydogan, H. Efeoglu, Semicond. Sci. Technol. 19 (2004) 242.
[17] M.K. Hudait, S.B. Krupanidhi, Solid State Electron. 44 (2000) 1089.
[18] M.Bh. Reddy, A.A. Kumar, V. Janardhanam, V.R. Reddy, P.N. Reddy, Curr. Appl. Phys. 9 (2009) 972.
[19] S.K. Cheung, N.W. Cheung, Appl. Phys. Lett. 49 (1986) 85.
[20] H. Uslu, A. Bengi, S.Ş. Çetin, U. Aydemir, Ş. Altındal, S.T. Aghaliyeva, S. Özçelik, J. Alloys Compd. 507 (2010) 190.
[21] Ş. Aydoğan, K. Çınar, H. Asıl, C. Çoşkun, A. Türüt, J. Alloys Compd. 476 (2009) 913.
[22] K. Ejderha, N. Yıldırım, B. Abay, A. Türüt, J. Alloys Compd. 484 (2009) 870.
[23] A. Tataroğlu, Ş. Altındal, J. Alloys Compd. 484 (2009) 405.
[24] A. Tataroğlu, Ş. Altındal, J. Alloys Compd. 479 (2009) 893.
[25] A. Sertap Kavasoglu, F. Yakuphanoglu, N. Kavasoglu, O. Pakma, O. Birgi, S. Oktik, J. Alloys Compd. 492 (2010) 421.
[26] A.A.M. Farag, A. Ashery, E.M.A. Ahmed, M.A. Salem, J. Alloys Compd. 495 (2010) 116.
[27] A.A.M. Farag, F.S. Terra, G.M. Mahmoud, A.M. Mansour, J. Alloys Compd. 481 (2009) 427.
[28] Ş. Altındal, A. Tataroğlu, İ. Dökme, Sol. Energ. Mater. Sol. Cell. 85 (2005) 345.
[29] S. Chand, J. Kumar, Semicond. Sci. Technol. 10 (1995) 1680.
[30] H.C. Card, E.H. Rhoderick, J. Phys. D: Appl. Phys. 4 (1971) 1589.
[31] P. Chattopadhyay, A.N. Daw, Solid State Electron. 29 (1986) 555.
[32] P. Cova, A. Singh, Solid State Electron. 33 (1990) 11.
[33] A. Singh, K.C. Reinhardt, W.A. Anderson, J. Appl. Phys. 68 (1990) 3475.
[34] Ö. Tüzün, Ş. Altındal, Ş. Oktik, Mat. Sci. Eng. B: Solid 134 (2006) 291.
[35] A. Tataroğlu, Ş. Altındal, M.M. Bülbül, Microelectron. Eng. 81 (2005) 140.
[36] W.E. Mahmoud, A.A. Al-Ghamdi, E. El-Tantawy, S. Al-Heniti, J. Alloys Compd. 485 (2009) 59.
[37] V. Janardhanam, H.L. Lee, K.H. Shim, H.B. Hong, S.H. Lee, J. Alloys Compd. 504 (2010) 146.
[38] E. Bacaksiz, G. Çankaya, İ. Polat, S. Yılmaz, C. Duran, M. Altunbaş, J. Alloys Compd. 496 (2010) 560.
[39] V. Janardhanam, A.A. Kumar, V.R. Reddy, P.N. Reddy, J. Alloys Compd. 485 (2009) 467.
[40] İ.Y. Erdoğan, Ö. Güllü, J. Alloys Compd. 492 (2010) 378.
[41] B. Abay, J. Alloys Compd. 506 (2010) 51.
[42] B. Güzeldir, M. Sağlam, A. Ateş, J. Alloys Compd. 506 (2010) 388.
[43] A. Yildiz, N. Serin, M. Kasap, T. Serin, D. Mardare, J. Alloys Compd. 493 (2010) 227.
[44] G.S. Chung, K.S. Kim, F. Yakuphanoğlu, J. Alloys Compd. 507 (2010) 508.
[45] F. Yakuphanoğlu, J. Alloys Compd. 470 (2010) 55.
[46] F. Yakuphanoğlu, M. Okutan, K. Korkmaz, J. Alloys Compd. 450 (2008) 39.
[47] H. Norde, J. Appl. Phys. 50 (1979) 5052.
[48] P. De Visschere, Solid State Electon. 29 (1986) 873.